Supplemental Material
Breaking the symmetry of momentum conservation using evanescent acoustic fields

Michael Mazilu,[1] Andriejus Demčenko,[2] Rab Wilson,[2] Julien Reboud,[2] and Jonathan M. Cooper[2]

[1]*SUPA, School of Physics and Astronomy, University of St Andrews, St Andrews, KY16 9SS, UK*
[2]*Division of Biomedical Engineering, School of Engineering, Rankine Building, Oakfield Avenue,The University of Glasgow, Glasgow, G12 8LT, UK*

(Dated: November 5, 2018)

EVANESCENT AND PROPAGATING WAVE INTERACTION

Figure 1 shows the raw time domain signal and filtered signal using a narrowband finite impulse response bandpass filter of center frequency 10 MHz. Multiples of the non-linear signal were seen due to propagating normal to the surface of the solid as predicted by the analytical model, see Fig. 2. A small difference between the predicted direction and experimental arrangement occurred due to maximisation of the non-linear signal amplitude (manual adjustment of the angles θ).

The analytical modelling results ($\theta_1 = 31.5°$ and $\theta_2 = -20.8°$), Fig. 2, show that the non-linear interactions resulting in the generated wave of the longitudinal polarisation occurs between two transversal waves (one of the waves is evanescent and one is propagating) (SS:L interaction), and longitudinal (evanescent) and transversal (propagating) waves (LS:L interaction). The rest of possible interactions (LL:L,SL:L) including generation of the transversal wave at the sum frequency can be neglected due to low intensities. In the model we used the following material properties: linear material properties ($\lambda = 53.05$ GPa, $\mu = 27.36$ GPa, $\rho = 2780$ kgm^{-3}, $c_f = 1481$ ms^{-1} and $\rho_f = 1000$ kgm^{-3}) we determined experimentally and non-linear properties from reference [14].

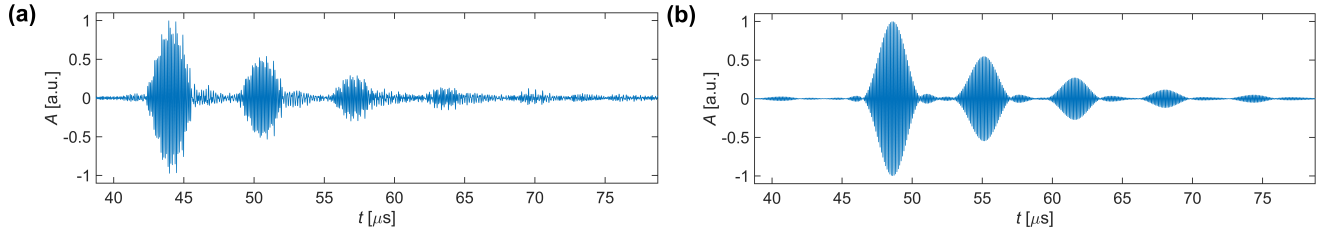

FIG. 1. Measured time-domain signal in a raw format (a) and filtered signal (b) when $x = 14$ mm.

Numerical modelling of submersed aluminium plate thickness was 5 mm, width was 20 mm was conducted using a 2D FE model implemented in COMSOL Multiphysics® v. 5.2a. Ultrasonic signals were collected in the fluid 1 mm below the solid specimen. Numerical result is shown in Fig. 3.

NON-LINEAR STRESS TENSOR

The non-linear stress tensor is given by:

$$\begin{aligned}\sigma_{ij}(\mathbf{v}) = (\mu + A/4)\left(\frac{\partial v_s}{\partial x_i}\frac{\partial v_s}{\partial x_j} + \frac{\partial v_i}{\partial x_s}\frac{\partial v_j}{\partial x_s} + \frac{\partial v_i}{\partial x_s}\frac{\partial v_s}{\partial x_j}\right)\\ + \frac{A}{4}\frac{\partial v_s}{\partial x_i}\frac{\partial v_j}{\partial x_s} + C\frac{\partial v_s}{\partial x_s}\frac{\partial v_r}{\partial x_r}\delta_{ij}\\ + \frac{B+\lambda}{2}\left(\frac{\partial v_s}{\partial x_r}\frac{\partial v_s}{\partial x_r}\delta_{ij} + 2\frac{\partial v_i}{\partial x_j}\frac{\partial v_s}{\partial x_s}\right)\\ + \frac{B}{2}\left(\frac{\partial v_s}{\partial x_r}\frac{\partial v_r}{\partial x_s}\delta_{ij} + 2\frac{\partial v_j}{\partial x_i}\frac{\partial v_s}{\partial x_s}\right),\end{aligned} \tag{1}$$

where δ_{ij} is the Kronecker delta symbol, A, B, C are the third order elastic constants. We assume here summation over repeated indices.

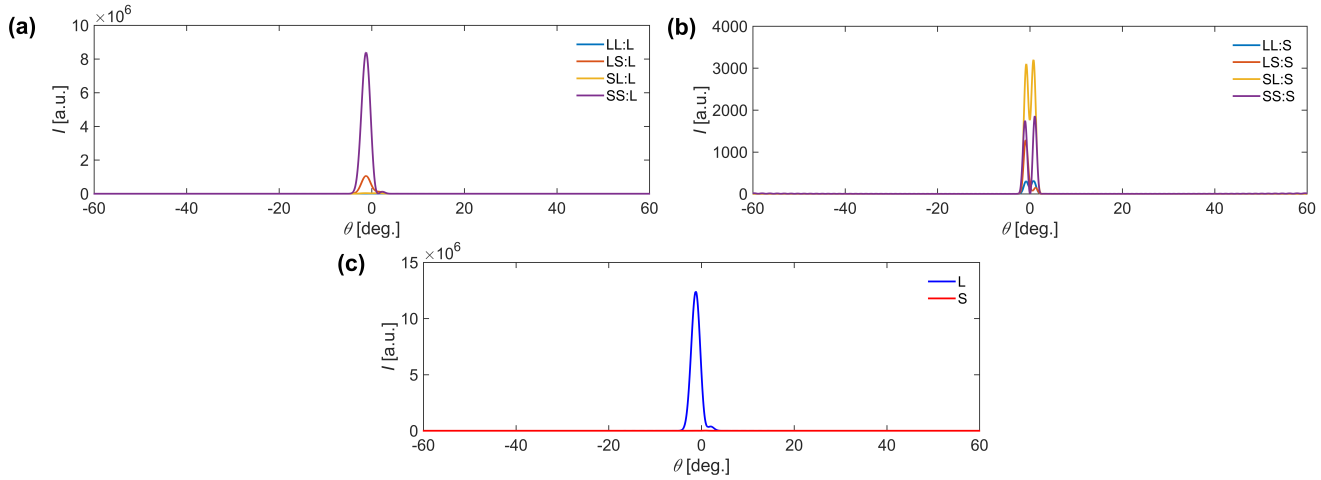

FIG. 2. Calculated angular intensity dependence at the sum-frequency wave generation for the 31.5° and −20.8° incidence angles: (a) the longitudinal wave polarisation, (b) the transversal wave polarisation, and (c) the total intensity with the maximum at −1.2° in the solid.

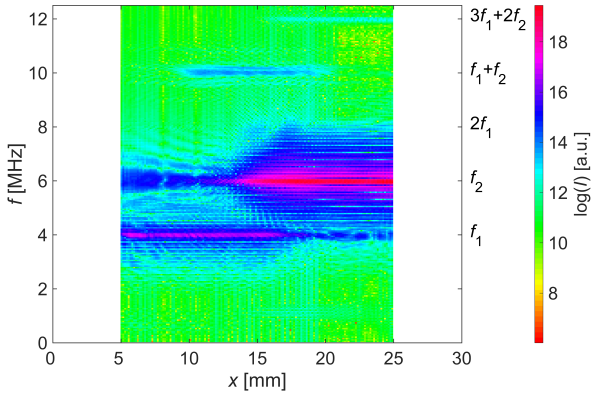

FIG. 3. Modelled sum frequency generation at the interface.

DIFFERENCE BETWEEN ACOUSTIC AND OPTICAL NON-LINEAR TERMS

To highlight the differences between the acoustic and the optical non-linear terms we use a Gaussian pulse traveling in the z-direction as a test displacement:

$$\mathbf{v} = \mathbf{u} e^{-\mathbf{r}\cdot\mathbf{r}/w^2} e^{-\mathrm{i}(\omega t - \mathbf{k}\cdot\mathbf{r})}, \tag{2}$$

where w is the pulse width and $\mathbf{u}$ is parallel to the wave-vector $\mathbf{k} = (0, 0, k_z)$. In this case, the non-linear force density in the propagation direction z is defined by

$$\begin{aligned}
f_z &= \mathbf{e}_z \cdot (\nabla \cdot \sigma_{ij}(\mathbf{v})) \\
&= v_z^2 \big(\mathrm{i}k_z^3(2A + 6B + 2C + 3\lambda + 6\mu) \\
&\quad + \frac{2\mathrm{i}}{w^2} k_z (8B + 2C + 5(\lambda + 2\mu)) + 6k_z(A(\mathrm{i} + 2k_z z) + k_z z(6B + 2C + 3\lambda + 6\mu)) \\
&\quad - \frac{2\mathrm{i}}{w^4}(6\mathrm{i}Az + 4Cz(\mathrm{i} + 3k_z z) + 3Ak_z(x^2 + y^2 + 4z^2) + 2B(8\mathrm{i}z + 3k_z(x^2 + y^2 + 6z^2))) \\
&\quad - \frac{2\mathrm{i}}{w^4}(2(5\mathrm{i}z + 3k_z(x^2 + y^2 + 3z^2))(\lambda + 2\mu)) \\
&\quad - 4z(3A(x^2 + y^2) + 4Az^2 + 4Cz^2 + 6B(x^2 + y^2 + 2z^2) + 6(x^2 + y^2 + z^2)(\lambda + 2\mu))\big)
\end{aligned}$$

where $\mathbf{e}_z$ is the unit vector in the z-direction. When the pulse width tends to infinity, this longitudinal force density tends to:

$$\lim_{w\to\infty} f_z = v_z^2 \mathrm{i} k_z^3 (2A + 6B + 2C + 3\lambda + 6\mu) \tag{3}$$

which corresponds to equation (3) in the main paper. However, for finite beams and finite pulses, the coefficient between f_z and v_z^2 depends on the position and the beam width/size. This implies that, contrary to non-linear optics where higher order susceptibilities can be used, in acoustics it is impossible to define a power-series expansion of the non-linear force as a function of the displacement.

NON-LINEAR QUADRATIC FUNCTION

To determine the bulk force resulting from the non-linear interaction of two plane waves with an output wave of a combined frequency, we considered the non-linear quadratic response function $g(w) = w^2$, defining $g_{12}(w_1, w_2) = (g(w_1 + w_2) - g(w_1 - w_2))/4 = w_1 w_2$ as a two-wave interaction term. The response function of any superposition between waves was then expressed as a sum of these two-wave interaction terms g_{12}. This methodology enabled the isolation of the different frequency mixing cases. A similar procedure can be implemented in the case of Hermitian expressions [18]for quadratic dependencies.

BULK NON-LINEAR FORCE

The bulk non-linear force is given by:

$$\nabla \cdot \sigma^{(12)} = \mathbf{F}^{(12)} = e^{-\mathrm{i}(\omega_1 t - \mathbf{k_1}\cdot\mathbf{r})} e^{-\mathrm{i}(\omega_2 t - \mathbf{k_2}\cdot\mathbf{r})} \mathbf{f}^{(12)}(\mathbf{u_1}, \mathbf{k_1}, \mathbf{u_2}, \mathbf{k_2}), \tag{4}$$

where

$$\begin{aligned}
\mathbf{f}^{(12)}(\mathbf{u_1}, \mathbf{k_1}, \mathbf{u_2}, \mathbf{k_2}) \;=\; & \mathrm{i}\tfrac{4\mu + A}{8} && ((\mathbf{u_1}\cdot\mathbf{u_2})(\mathbf{k_2}\cdot(\mathbf{k_1}+\mathbf{k_2}))\mathbf{k_1} + (\mathbf{u_1}\cdot\mathbf{u_2})(\mathbf{k_1}\cdot(\mathbf{k_1}+\mathbf{k_2}))\mathbf{k_2} \\
& && +(\mathbf{k_1}\cdot\mathbf{k_2})(\mathbf{u_1}\cdot(\mathbf{k_1}+\mathbf{k_2}))\mathbf{u_2} + (\mathbf{k_1}\cdot\mathbf{k_2})(\mathbf{u_2}\cdot(\mathbf{k_1}+\mathbf{k_2}))\mathbf{u_1} \\
& && +(\mathbf{u_1}\cdot\mathbf{k_2})(\mathbf{k_1}\cdot(\mathbf{k_1}+\mathbf{k_2}))\mathbf{u_2} + (\mathbf{u_2}\cdot\mathbf{k_1})(\mathbf{k_2}\cdot(\mathbf{k_1}+\mathbf{k_2}))\mathbf{u_1}) \\
& +\mathrm{i}\tfrac{A}{8} && ((\mathbf{u_1}\cdot\mathbf{k_2})(\mathbf{u_2}\cdot(\mathbf{k_1}+\mathbf{k_2}))\mathbf{k_1} + (\mathbf{u_2}\cdot\mathbf{k_1})(\mathbf{u_1}\cdot(\mathbf{k_1}+\mathbf{k_2}))\mathbf{k_2}) \\
& +\mathrm{i}\tfrac{B+\lambda}{2} && ((\mathbf{u_1}\cdot\mathbf{u_2})(\mathbf{k_1}\cdot\mathbf{k_2})(\mathbf{k_1}+\mathbf{k_2}) + (\mathbf{u_2}\cdot\mathbf{k_2})(\mathbf{k_1}\cdot(\mathbf{k_1}+\mathbf{k_2}))\mathbf{u_1} \\
& && +(\mathbf{u_1}\cdot\mathbf{k_1})(\mathbf{k_2}\cdot(\mathbf{k_1}+\mathbf{k_2}))\mathbf{u_2}) \\
& +\mathrm{i}\tfrac{B}{2} && ((\mathbf{u_1}\cdot\mathbf{k_1})(\mathbf{u_2}\cdot\mathbf{k_2})(\mathbf{k_1}+\mathbf{k_2}) + (\mathbf{u_1}\cdot\mathbf{k_2})(\mathbf{u_2}\cdot(\mathbf{k_1}+\mathbf{k_2}))\mathbf{k_1} \\
& && +(\mathbf{u_2}\cdot\mathbf{k_1})(\mathbf{u_1}\cdot(\mathbf{k_1}+\mathbf{k_2}))\mathbf{k_2}) \\
& +\mathrm{i}C && (\mathbf{u_1}\cdot\mathbf{k_1})(\mathbf{u_2}\cdot\mathbf{k_2})(\mathbf{k_1}+\mathbf{k_2}).
\end{aligned} \tag{5}$$

Then

$$\begin{aligned}
\nabla \cdot \sigma_{ij}(\mathbf{v}) &= 2\mathbf{f}^{(12)}(\mathbf{u_1}, \mathbf{k_1}, \mathbf{u_2}, \mathbf{k_2}) e^{\mathrm{i}(\omega_1 t - \mathbf{k_1}\cdot\mathbf{r})} e^{\mathrm{i}(\omega_2 t - \mathbf{k_2}\cdot\mathbf{r})} + c.c. \\
&= 2\mathbf{f}^{(12)}(\mathbf{u_1}, \mathbf{k_1}, \mathbf{u_2}, \mathbf{k_2}) e^{\mathrm{i}(\omega_1 t - \mathbf{k_1}\cdot\mathbf{r})} e^{\mathrm{i}(\omega_2 t - \mathbf{k_2}\cdot\mathbf{r})} \\
&\quad - 2\mathbf{f}^{(12)}(\mathbf{u_1^*}, \mathbf{k_1^*}, \mathbf{u_2^*}, \mathbf{k_2^*}) e^{-\mathrm{i}(\omega_1 t - \mathbf{k_1^*}\cdot\mathbf{r})} e^{-\mathrm{i}(\omega_2 t - \mathbf{k_2^*}\cdot\mathbf{r})},
\end{aligned} \tag{6}$$

where * denotes the complex conjugate.

ANALYTICAL EXPRESSION OF VOLUME INTEGRAL

Equation (main text, 10) can be integrated in the volume ($\pm\Delta x$, $\pm\Delta y$ and $(0, -\Delta z)$) (non-linear medium positioned at $z = 0$ and waves propagate and/or evanescently decay for $z < 0$) and this leads to:

$$\begin{aligned} A_3 = {} & 2\Delta x\Delta y\Delta z \frac{a_1 a_2 \mathbf{u_3}\cdot\mathbf{f^{(12)}}(\mathbf{u_1},\mathbf{k_1},\mathbf{u_2},\mathbf{k_2})}{\mathrm{i}c_3\rho\omega_3} \\ & \times e^{\mathrm{i}(k_{1z}+k_{2z}-k_{3z})\Delta z/2} \\ & \times \mathrm{sinc}((k_{1x}+k_{2x}-k_{3x})\Delta x) \\ & \times \mathrm{sinc}((k_{1z}+k_{2z}-k_{3z})\Delta z/2) \\ & - 2\Delta x\Delta y\Delta z \frac{a_1^* a_2^* \mathbf{u_3}\cdot\mathbf{f^{(12)}}(\mathbf{u_1^*},\mathbf{k_1^*},\mathbf{u_2^*},\mathbf{k_2^*})}{\mathrm{i}c_3\rho\omega_3} \\ & \times e^{-\mathrm{i}(k_{1z}^*+k_{2z}^*+k_{3z})\Delta z/2} \\ & \times \mathrm{sinc}((k_{1x}^*+k_{2x}^*+k_{3x})\Delta x) \\ & \times \mathrm{sinc}((k_{1z}^*+k_{2z}^*+k_{3z})\Delta z/2). \end{aligned} \tag{7}$$

EXPERIMENTAL AND ANALYTICAL RESULTS FOR DIFFERENT WAVE INTERACTION CASES AT VARIOUS EXPERIMENTAL ARRANGEMENTS

The presented analytical model was verified by experiments at 3 different measurement conditions when beams of the initial waves overlap on a surface of solid material (aluminium). The arrangements are noted as Case 1, Case 2 and Case 3 for further analysis. Figure 4 depicts experimental configuration and it's characteristic parameters such as incidence angles $\theta_{1,2}$ of the initial waves, a wave measurement angle θ_{R}, spatial parameters Δx and $\Delta z_{1,2,\mathrm{R}}$ for the arrangement of the sources S($f_{1,2}$) and the receiver R. Whilst parameter Δx_0 shows the offset of the intersection of the center beams on the solid surface from the x axis origin.The actual measurement parameters are listed in Table I.

Case 1 and 2 enabled non-linear interactions between propagating and evanescent waves. Case 3 was dedicated to interactions between evanescent waves only. Figures 5 and 6 depict measured ultrasonic fields and corresponding raw and filtered time-domain signals for all 3 cases, respectively. Multiples of the sum frequency signal are seen in Figs. 6(a) and (b) for Case 1. Figures 6(a) and (b) show that the strong first signal with a small re-reflected signal was detected in the wave mixing experiment due to the rotated (from the normal) propagation direction of the generated wave in Case 2. Only the first signal was detected in Case 3 due to the significantly rotated propagation direction of the sum frequency wave.

Figure 7 shows results of the analytical model for the three wave mixing cases. The results show, Figs. 7(a) and (b), that the interactions SS:L and SL:L are dominant in the wave-mixing. Other possible interactions can be ignored due to their low intensities. A difference between experimentally measured and predicted wave propagation angle is observed due to maximisation of the non-linear wave signal. The measured non-linear wave signal traces from $x = 0$ mm to $x = 10$ mm, see Fig. 5(a), shows that the wave propagation direction was not ideally normal to the surface of the solid material.

Figures 7(d) and (e) depict the dominant interactions in the wave mixing experiment for Case 2. The results show that the SS:L interaction is the dominant and other interactions can be excluded from the analysis in this case.

The calculated results for Case 3 are shown in Figs. 7(g)-(i). The results show that the non-linear wave interactions between two initial evanescent waves are supported by all 4 interactions (LL:L, LS:L, SL:L and SS:L) in the longitudinal wave generation case. The transversal wave generation was also sported by all 4 interactions (LL:S, LS:S, SL:S and SS:S). In both cases (longitudinal and transversal waves) the interaction between two evanescent waves was the strongest. The weakest interaction was between two evanescent longitudinal waves. It is important to note that in Case 3 the intensities of the generated waves (longitudinal and transversal) were of the same order. Nevertheless that these two waves propagate at two different directions in the solid, these waves have single propagation direction after refraction from the solid to fluid. Hence, both components are present in the measured data.

The analytical model shows (Fig. 7) that the maximum intensity of the generated longitudinal wave is expected at 26° in the solid. This well agrees with the experimentally determined angle which is 26° (calculated from the Snell's law). Due to the large rotation angle only the first signal is detected by the receiver, see Figs. 6(e) and (f).

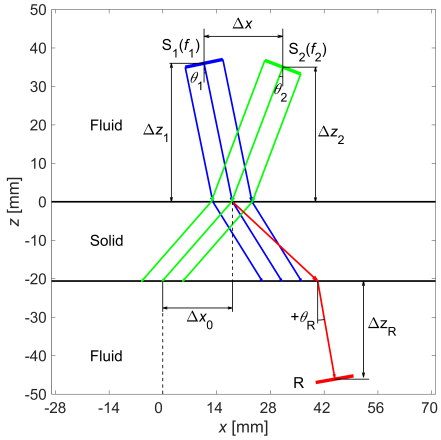

FIG. 4. Experimental arrangement for the non-linear wave mixing of propagating and evanescent waves at the sum frequency, where $S_{1,2}$ are the sources of initial waves, R is the receiver of the center frequency 10 MHz.

TABLE I. Experimental parameters used in the non-linear wave mixing experiments.

Case	θ_1 [deg.]	θ_2 [deg.]	θ_R [deg.]	Δx [mm]	Δx_0 [mm]	Δz_1 [mm]	Δz_2 [mm]	Δz_R [mm]	f_1 [MHz]	f_2 [MHz]
1	11.6	-20.8	-1	20.5	18.1	36	35	25	6	4
2	24.8		-2	22	22.8	26	27		4	6
3	30.6	-30.1	+6	31	3	27			6	4

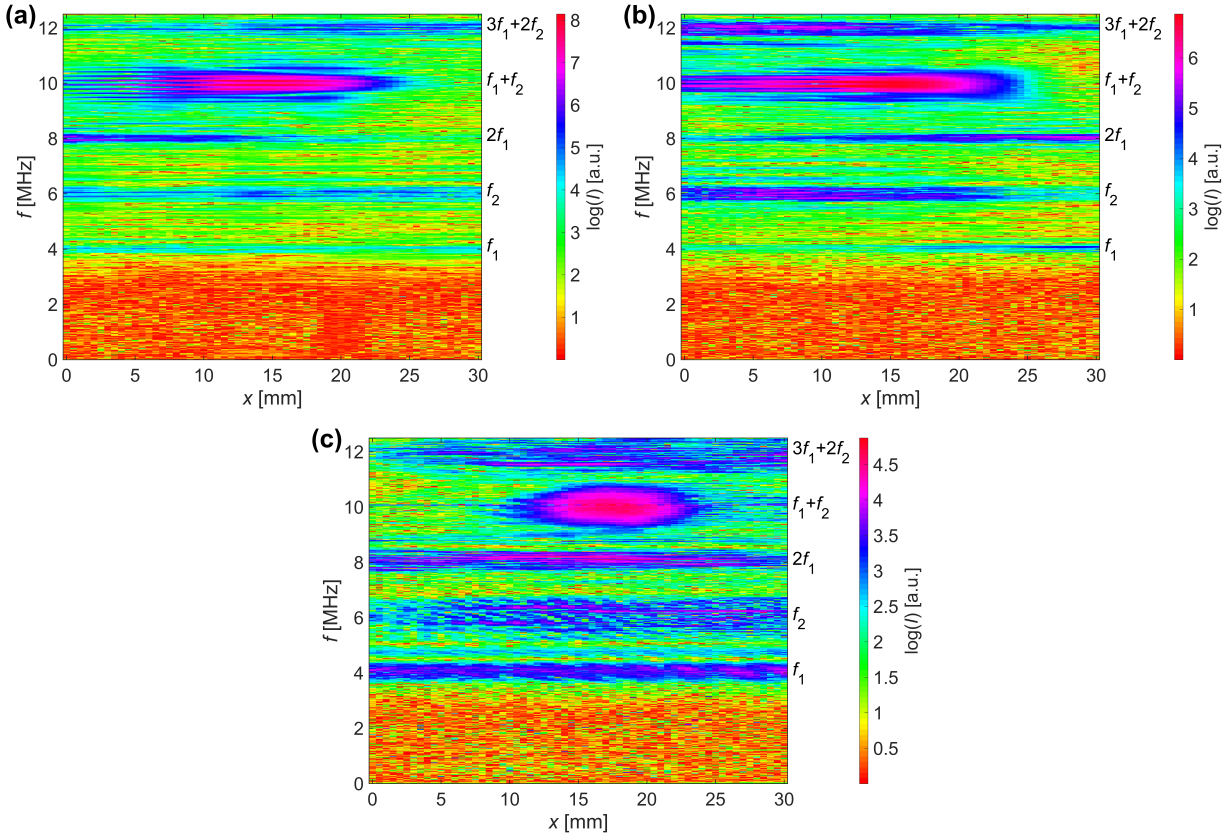

FIG. 5. Measured sum frequency generation at the interface for: (a) Case 1, (b) Case 2, and (c) Case 3.

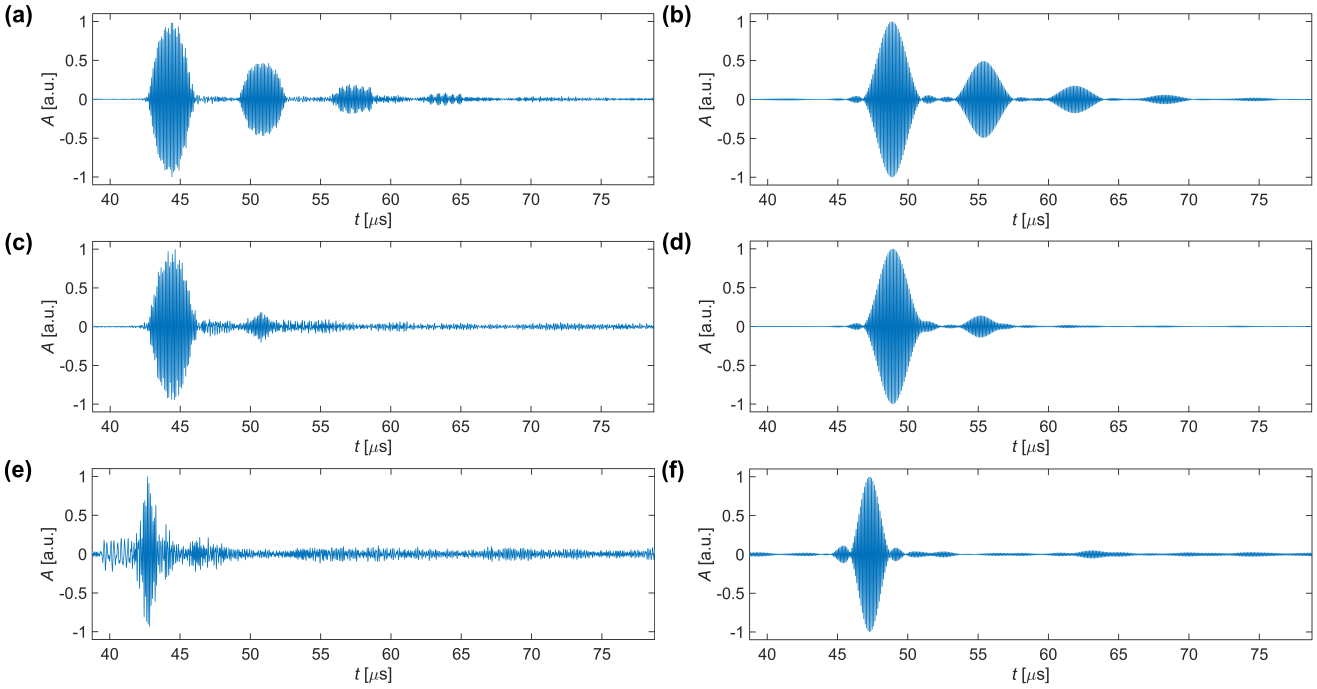

FIG. 6. Measured time-domain signals in a raw format (a), (c) and (e), and filtered signals (b), (d) and (f). The shown signals correspond to the wave mixing experiments: (a) and (b) Case 1 when $x = 15$ mm, (c) and (d) Case 2 when $x = 15$ mm, (e) and (f) Case 3 when $x = 17$ mm.

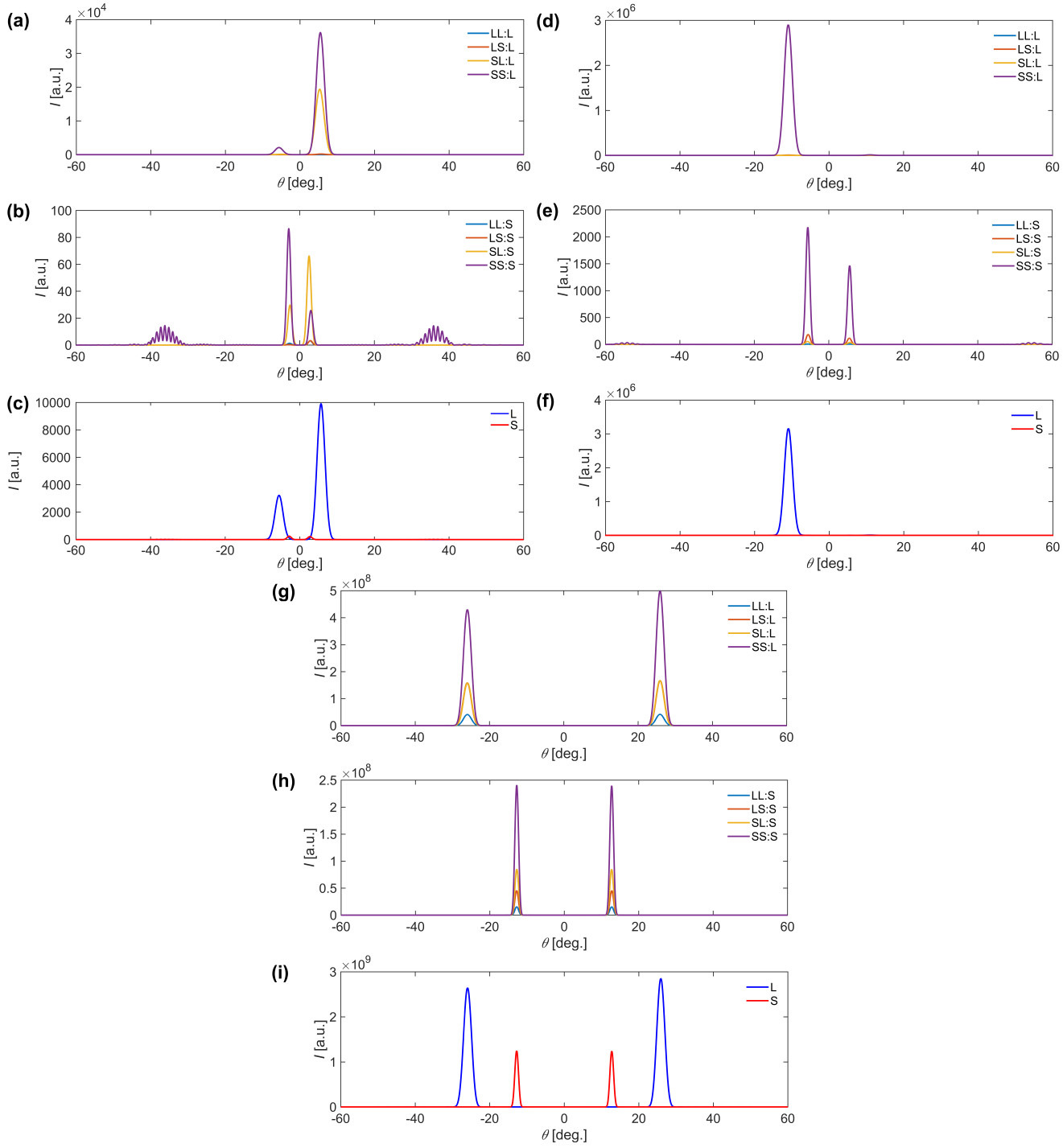

FIG. 7. Calculated angular intensity dependence at the sum-frequency wave generation for: (a)-(c) Case 1 with total intensity maximum at 5.6° in the solid, (d)-(f) Case 2 with total intensity maximum at 10.9° in the solid, and (g)-(i) Case 3 with total intensity maximum at 26° in the solid.